Study on forward-running detonation drivers for high enthalpy shock tunnels

Z.L. Jiang*, W. Zhao*, C. Wang* and K. Takayama**

*LHD, Institute of Mechanics, Chinese Academy of Sciences,
Beijing 100080, China; zljiang@imech.ac.cn and wzhang@imech.ac.cn
**Shock Wave Research Center, Institute of Fluid Science, Tohoku University,
2-1-1 Katahira, Aoba-ku, Sendai 980-8577, Japan; e-mail: takayama@ifs.tohoku.ac.jp

Abstract. In order to improve the quality of driving flows generated with detonation-driven shock tunnels operated in the forward-running mode, various detonation drivers with specially-designed sections were examined in this paper. Four configurations of the specially-designed section, three with different converging angles and one with a cavity ring, were simulated by solving the Euler equations implemented with a pseudo-kinetic reaction model. From the first three cases, it is observed that the reflection of detonation fronts at the converging wall results in an upstream travelling shock wave that can increase the flow pressure that has decreased due to expansion waves, which leads to improvement of the driving flow. The configuration with a cavity ring is found to be more promising since the upstream travelling shock wave appears stronger and the detonation front is less overdriven. Although pressure fluctuations due to shock wave focusing and shock wave reflection are observable in these detonation drivers, they attenuate very rapidly to an acceptable level as the detonation wave propagates downstream. Based on the numerical observations, a new detonation-driven shock tunnel with a cavity ring is designed and installed for experimental investigation. Experimental results confirm the conclusion drawn from numerical simulations. and the generated driving flow in this shock tunnel could maintain uniformity for as long as 4 ms. Feasibility of the proposed detonation driver for high enthalpy shock tunnels is well demonstrated.

1 Introduction

From the beginning of the last century, aerodynamic research has been driven by the urge to fly faster and higher. So far, supersonic flight has been achieved and the new century is expected to be the era of practical hypersonic flight. The urge poses many exciting challenges to aerodynamic scientists and engineers. The development of high enthalpy shock tunnels for reliable ground testing of hypersonic vehicles is one of these research topics. It is because for flight speeds higher than Mach 8, that is, at high stagnation enthalpies, there exist technological barriers which would be very hard to overcome with the blowdown-type hypersonic wind tunnels. Therefore, shock tunnels become the facilities of choice for high enthalpy ground testing. So far as their operation concepts are concerned, two major kinds

of the shock tunnels are widely applied to generate high enthalpy test flows: one is driven by a free-piston and the other by gaseous detonation.

The concept of the free-piston driver was studied as early as 1959 at NRC in Ottawa, Canada, and the work was reported later by Stalker[1] in 1961. A series of free-piston shock tunnels was then initiated in Australia and the first such facility was realized by modifying a conventional shock tunnel[2]. Within the next three decades, many free-piston-driven shock tunnels have been constructed and installed over the world, such as T2 and T3 at the Australian National University, Australia, T4 at the University of Queensland, Australia, T5 at the California Institute of Technology, USA, HEG at Göttingen, Germany, and HEK and HiEST at the National Aerospace Laboratory at Kakuda, Japan [3-8]. These shock tunnels are widely used to generate high enthalpy test flows with effective test time ranging from 0.1 to 2.0ms.

An alternate technique is the so-called detonation driver in which the driver gas is generated by the detonation of a gaseous reactive mixture. As early as 1957, Bird[9] studied the wave processes in the detonation driver and its superior performance compared to the conventional shock driver. Since then several detonation-driven shock tunnels have been constructed and put into operation. Yu et al. had developed a detonation-driven shock tube in the backward running mode at the Institute of Mechanics in Beijing[10,11] and later modified it to be a shock tunnel[12]. Meantime, a shock tunnel of 140 mm diameter was constructed at the the Shock Wave Laboratory, RWTH Aachen, Germany, which was largely performed as a joint research project with the Institute of Mechanics, Chinese Academy of Sciences[13]. In addition, two detonation-driven shock tunnels configured in the forward-running mode are in operation at GASL in New York and at The University of Texas at Arlington, USA[14]. The effective test time achieved with the detonation-driven shock tunnels can be as long as 4.0ms.

Comparing the detonation-driven shock tunnels with free-piston driven one, one could see that the detonation-driven shock tunnel is easier to operate with a relatively longer test time and lower operation cost. However, before completing this technology, the problems related to the fundamental physics of detonation and the assessment of its application to high enthalpy shock tunnels have to be investigated.

In order to explain the operational concept of detonation drivers, it is helpful to recall the Chapman-Jouguet theory[15,16] (the C-J theory) and the Taylor similarity law[17], which have proved to describe well the global features of gaseous detonation. Assuming that a tube closed at one end is filled with a detonable gas mixture at rest and the detonation is initiated at its closed end. The wave motion can be described by the C-J theory and the Taylor similarity law. In this wave system, the detonation front is taken as a shock wave propagating into the unburned detonable gas mixture, which compresses the gas mixture ahead of it and elevates the gas pressure and temperature so high as to initiate an auto-ignition. Hence, a chemical reaction concurrently takes place in an infinitely thin reaction zone, and then the burned gas reaches to the state that can be determined with the C-J condition which states that behind the reaction zone, there is a plane in which the velocity of gas particles of the detonation product relative to the wave front is equal to the local
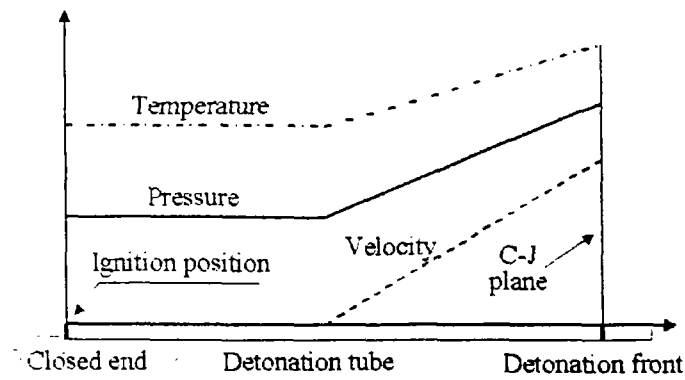
96

Fig.1 Distributions of detonation wave properties along the length of a detonation tube, the problem described with the Taylor similarity law[17]

speed of sound. Behind this C-J plane the flow expands to a steady state at zero velocity and the uniform pressure being about 40% of the C-J pressure. The length of the flow in the uniform state is about half of the distance in which the detonation wave has propagated. The distributions of detonation wave properties along the length of the detonation tube are schematically presented in Fig. 1, and this figure will be used to discuss further the operating concept of detonation-driven shock tunnels.

If a driven section is connect to the left of the detonation tube as shown in Fig. 1, the tail of the Taylor expansion wave is utilized as the high pressure driver gas[12,13]. This operational concept is referred to as the backward-running mode because the detonation front propagates upstream, instead of in the direction of the flow in the driven (or shock) tube. A uniform driving flow is obtainable in this mode, but the driving pressure and temperature so far achievable is not so high as that created with a heavy free-piston compression because of the pressure limitation of detonation tube materials. From the detonation properties presented in Fig. 1, it is known that the driver gas pressure is only about 40% of the C-J pressure and the kinetic energy of the gas flow is zero. This leads to another way to drive the test gas in the driven section by connecting the driven section to the right of the detonation tube: this mode of operation is named the forward-running mode. That is, the detonation propagates forward in the direction of the primary shock propagation in the driven section. It is obvious that a driving flow of much higher stagnation pressure could be obtainable but it is not very uniform due to the Taylor expansion behind the detonation front.

In order to overcome the deficiency of the detonation driver operated in the forward-running model, several detonation drivers with a specially-designed section were proposed in this paper. The basic idea is to add this section to the conventional detonation driver so that an upstream-travelling shock wave could be generated to increase the flow pressure that has decreased due to expansion waves. Three types of detonation drivers, as sketched in Fig. 2, are numerically investigated to examine the driving flow uniformity. The first type of detonation driver consists of a large diameter tube, a small diameter tube, and a converging section between them, as shown in Fig. 2a. Two configurations are obtained by
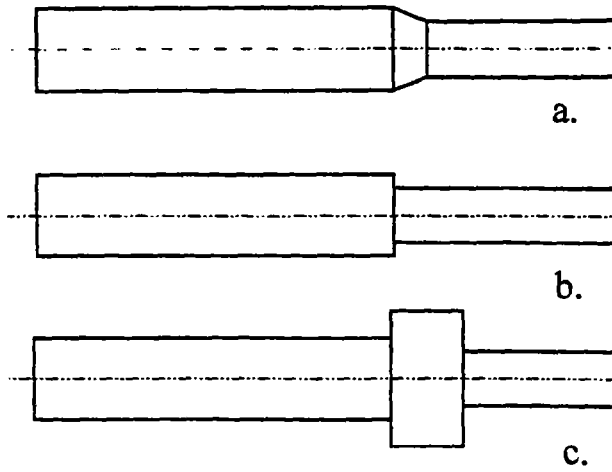
97

Fig.2 Schematic configurations of detonation drivers proposed for numerical investigation

varying the convergence angle from 30° to 45°. The second type of detonation driver. as shown in Fig. 2b, is similar to the first one but without the converging section. Actually. this type can be achieved by increasing the convergence angle of the first type to 90°. In the third type of detonation driver, as shown in Fig. 2c, the converging section is replaced by a cavity ring.

By solving the Euler equations for a binary mixture of perfect gases implemented with a pseudo-kinetic reaction model[18], numerical simulations of four cases are carried out to investigate the effects of various configurations on the driving flow uniformity. It is found that the detonation drivers with converging sections do improve the driving flow uniformity, but the one with a cavity ring shows more promising characters. According to the numerical investigation. a detonation-driven shock tunnel with a cavity ring is manufactured and installed at the Institute of Mechanics, Chinese Academy of Sciences, Beijing. Some experiments were conducted and pressure histories (pressure variations against time) were measured at the end wall of the driven section. The experimental data confirm the numerical investigation. which shows that multiple shock reflections resulting from the specially-designed section lead to the generation of an upstream-travelling shock wave that can increase the flow pressure behind the detonation front and help to create a uniform test gas slug.

2 Governing equations and numerical methods

The flow phenomena concerned in this paper are the wave dynamic processes in which viscosity effects are negligible. The two-dimensional Euler equations in conservation form for a binary mixture of the perfect gases are written in cylindrical coordinates as

$$\frac{\partial U}{\partial t} + \frac{\partial F}{\partial x} + \frac{\partial G}{\partial r} + \frac{1}{r}S = H. \qquad (1)$$

98

where (x, r, t) are the coordinates and time. **U**, **F**, **G**, **S** and **H** denote the state variables, fluxes and sources, respectively, and are given by

$$
\mathbf{U} = \begin{pmatrix} \rho_1 \\ \rho_2 \\ \rho u \\ \rho v \\ e \end{pmatrix}, \quad
\mathbf{F} = \begin{pmatrix} \rho_1 u \\ \rho_2 u \\ \rho u^2 + p \\ \rho u v \\ (e+p)u \end{pmatrix}, \quad
\mathbf{G} = \begin{pmatrix} \rho_1 v \\ \rho_2 u \\ \rho u v \\ \rho v^2 + p \\ (e+p)v \end{pmatrix},
$$

$$
\mathbf{S} = \begin{pmatrix} \rho_1 v \\ \rho_2 u \\ \rho u v \\ \rho v^2 \\ (e+p)v \end{pmatrix}, \quad
\mathbf{H} = \begin{pmatrix} \rho h(\rho_1, \rho_2, p) \\ -\rho h(\rho_1, \rho_2, p) \\ 0 \\ 0 \\ 0 \end{pmatrix}, \tag{2}
$$

where the primitive variables in the unknown **U** are density ρ: the reactant density ρ_1; the product density ρ_2; velocity components u and v in $x-$ or y-direction, respectively; the reaction rate $h(\rho_1, \rho_2, p)$; and total energy per unit mass e, related to the equation of state for the perfect gaseous mixture by

$$
e = \frac{p}{\gamma - 1} + \frac{1}{2}\rho(u^2 + v^2) + \rho_1 Q, \tag{3}
$$

where Q is the chemical reaction heat release per unit mass. It is assumed that the equation of state is independent of the composition of gas mixtures, but the internal specific energy is modified to include the latent heat of combustion. The density of the gas mixture is calculated by

$$
\rho = \rho_1 + \rho_2. \tag{4}
$$

If mass fractions are denoted by $Z_1 = \rho_1/\rho$ and $Z_2 = \rho_2/\rho$, the effective adiabatic exponent of the gas mixture. γ, can be put in the form

$$
\gamma = \frac{\dfrac{Z_1\gamma_1}{m_1(\gamma_1 - 1)} + \dfrac{Z_2\gamma_2}{m_2(\gamma_2 - 1)}}{\dfrac{Z_1}{m_1(\gamma_1 - 1)} + \dfrac{Z_2}{m_2(\gamma_2 - 1)}}, \tag{5}
$$

where γ_1 and m_1 are the adiabatic exponent and molecular weight for the reactant, and γ_2 and m_2 are the respective parameters for the product. The governing equations, Eqs. (1), are discretized using a dispersion-controlled scheme proposed by Jiang et al[19]. The time-marching integration is performed using a Runge-Kutta integration method of second-order accuracy. The computational mesh uses an equally-spaced Cartesian grid to accommodate the oblique rigid wall, where the ratio of mesh size $\Delta y/\Delta x$ is chosen so that the oblique wall could coincide with the cell diagonal. This choice enables a simple and accurate algorithm to be implemented with our scheme, producing a rigid wall boundary condition of second-order accuracy through computing the "mirror-image" flow states at virtual grid points outside the wall. A 5000×30 mesh system is generated to cover the detonation driver of 5 m in length and 60 mm in diameter. The mesh size is 1 mm wide and its length is adjustable according to the given convergence angle.

99

3 Reaction model

In order to examine gas dynamic characteristics of a detonation driver, the entire detonation tube has to be simulated. The mesh size that could be used, as mentioned in the last section, is still too large to capture accurately either the detonation structure or the thickness of detonation front because of the large length-to-diameter ratio. Therefore, the strategy for selecting a kinetic reaction rate model is to obtain an idealized the Taylor expansion wave having an infinitely thin reaction zone. The emphasis here is to predict the gas dynamics in front of and following a detonation front, rather than to correctly produce either the detailed detonation structure or the process by which a shock wave propagating in the reactive gas mixture evolves gradually into a detonation wave. The following pseudo-kinetic reaction rate[18] has been proved to be acceptable for our purposes:

$$h(\rho_1, \rho_2, p) = \begin{cases} 0 & p < P_{ignit} \\ -Adet(\frac{D_{CJ}}{\Delta s})(\frac{p}{P_{CJ}})^\alpha Z_1^\beta & \text{otherwise} \end{cases} \quad (6)$$

where D_{CJ} is the C-J velocity; P_{CJ} is the C-J pressure; Δs is the local mesh size; P_{ignit} is an ignition pressure; $Adet$, α, β are dimensionless constants of order unity whose values are determined by inspecting one-dimensional simulations of detonation and looking for the captured solutions close to the Taylor similar solutions and the C-J conditions, which are known to predict well the global features of gaseous detonation. A set of values for these constants was determined by such a procedure and is given below[18]. These constants depend mainly on the gas mixture and vary slightly with numerical schemes. Once tuned they keep constant throughout computation.

$$\begin{cases} P_{ignit} = 0.4P_{CJ}, \\ \alpha = 1.0, \\ \beta = 0.5, \\ Adet = 1.6. \end{cases} \quad (7)$$

All the computational results presented in this paper have been produced with this set of "tuned" constants of the pseudo-kinetic reaction model. Validation of calculated results with this model has been carried out by comparing with experimental data, the maximum discrepancy in the C-J velocity, pressure and Mach number is less than 5%[18], which is an acceptable level for our purpose of analyzing the wave dynamic processes. However, while this reaction model is capable of describing the flow features as presented by the Taylor similarity law, the von Neumann spike (or shock pressure) can not be captured even if the mesh size were sufficiently fine. A more detailed reaction model could have been used to simulate the detonation structure and its associated shock pressure, but it would also consume much of the computational resources. And although the current model does not include the reaction zone in the detonation, it nevertheless contains the essential qualitative features of the propagating wave and is still a useful tool for the current parametric study.

4 Numerical results and discussion

Using the governing equations, the numerical methods and the chemical reaction model introduced in the previous sections, the three types of the detonation drivers (see Fig. 2) are simulated to examine the wave interaction in the specially-designed section and its effects on the driving flow. In these test cases, the detonation driver is about 5 m long in total and consists of three sections: two straight tubes with different diameters and a specially-designed area-changing section between the two tubes. The detonative gas used in numerical simulations is a mixture of $2H_2 + O_2$ at the initial condition of $P_i = 1.0$ bar and $T_i = 298.15$ K. The adiabatic exponents are taken to be 1.402 for the reactants and 1.219 for the products. The reaction energy is $Q = 8.39 \times 10^6 (J/kg)$. The molecular weights are 12 for the reactants and 18 for the products.

In the following discussion, two major physical processes are emphasized. The first process is the wave interaction after the detonation front moves into the specially-designed section. Sequential isobars of the flow motion near the specially-designed section will be presented to show the wave propagation, reflection and focusing. The other is the pressure variations induced by the wave interaction on the driving flow. Sequential profiles of pressure distributions along the axis of symmetry in the detonation drivers are plotted for investigation. From these results, the observed wave phenomena are explained, the mechanism behind the phenomena is explored, and their effects on driving flows are discussed.

4.1 Detonation driver with a 30° convergence angle

The first case carried out is the configuration of type A as shown in Fig. 2a by setting a 30° convergence angle. For this case, the large straight tube is 3.5 m long and 90 mm in diameter. and the small tube is 1.5 m long and 60 mm in diameter. Between these two tubes, a section with a 30° convergence angle is inserted. Numerical results are plotted in Figs. 3 and 4.

Figure 3 shows four time sequences of isobars of the flow motion shortly before and after the detonation front moves into the converging section. Time interval is 25 μs between Figs. 3a. 3b and 3c. and 50 μs between Figs. 3c and 3d. Firstly, a planar detonation wave (i.e., the front of the Taylor expansion wave) as observed in Fig. 3a arrives at the entrance of the converging section, behind which expansion waves are observable from the isobar as annotated. The detonation wave front reflects from the converging wall in Fig. 3b. and Mach reflections develop later. Wave diffraction is also observable behind the Mach stem as the expansion waves behind the detonation front pass through the converging section. Then. the reflected shock wave coalesces in Fig. 3c, and a nearly normal shock wave develops and propagates upstream, as shown in Fig. 3d. This shock wave can elevate both the pressure and temperature of the flow that has passed through the shock wave. At the same time. a downstream travelling shock wave is also generated and catches up with the detonation front very quickly as shown in Fig. 3c, which will result in an over-driven detonation front. Moreover, it is observable in Figs. 3c and 3d that transverse wave reflections repeatedly appear between the detonation front and the upstream travelling shock wave, which may
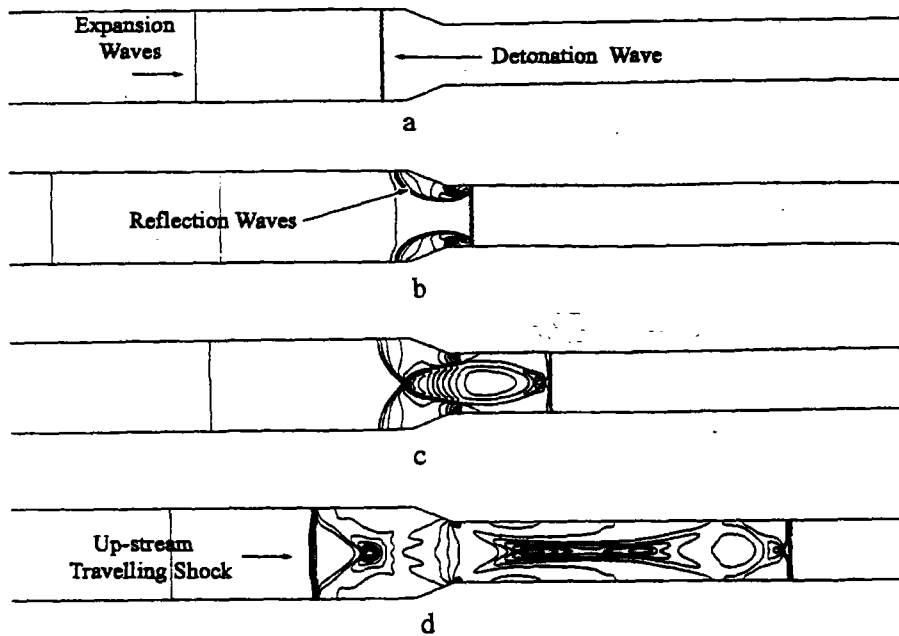
101

Fig. 3 Time sequences of isobars of the flow motion showing wave interactions in case one with a 30° converging angle

induce pressure fluctuations in this region.

Sequential pressure distributions along the axis of symmetry of case one are presented in Fig. 4 at four time steps to aid further discussion. Figure 4a corresponds to the time instant when a detonation front arrives at the entrance of the converging section, as shown in Fig. 3a. The typical pressure distribution of the Taylor expansion wave is observable here, which consists of the C-J plane in the detonation front, the expansion waves and a flow slug at uniform pressure. This result shows that the reaction model adopted here can represent well the Taylor similarity law. Figure 4b shows the flow state shortly after the reflected shock waves merge at the axis of symmetry as shown in Fig. 3c. Two pressure peaks appear in Fig. 4b: the higher one represents the post-shock pressure of the upstream travelling shock wave and the other represents the detonation front. The higher peak pressure is about 40 times higher than the initial pressure, but decreases very rapidly as the upstream travelling shock wave propagates forward, as seen in Figs. 4c and 4d. The pressure peak behind the detonation front is higher than the C-J pressure (see Fig. 4a), which means the detonation front is over-driven. The upstream travelling shock wave induces a pressure level that achieved an average value of 70% of the C-J pressure, as shown in Fig. 4d. Although the pressure fluctuations shown in Fig. 4c due to the repeatedly-reflected shock waves are rather higher, they attenuate quite quickly, as seen in Fig. 4d. This implies that a more uniform driving flow could be expected in the driven section. Furthermore, by comparing the pressure profile in Fig. 4a with that in Fig. 4d, it can be concluded that as a driving flow, the flow state in Fig. 4d is more preferable than in Fig. 4a, therefore, the converging
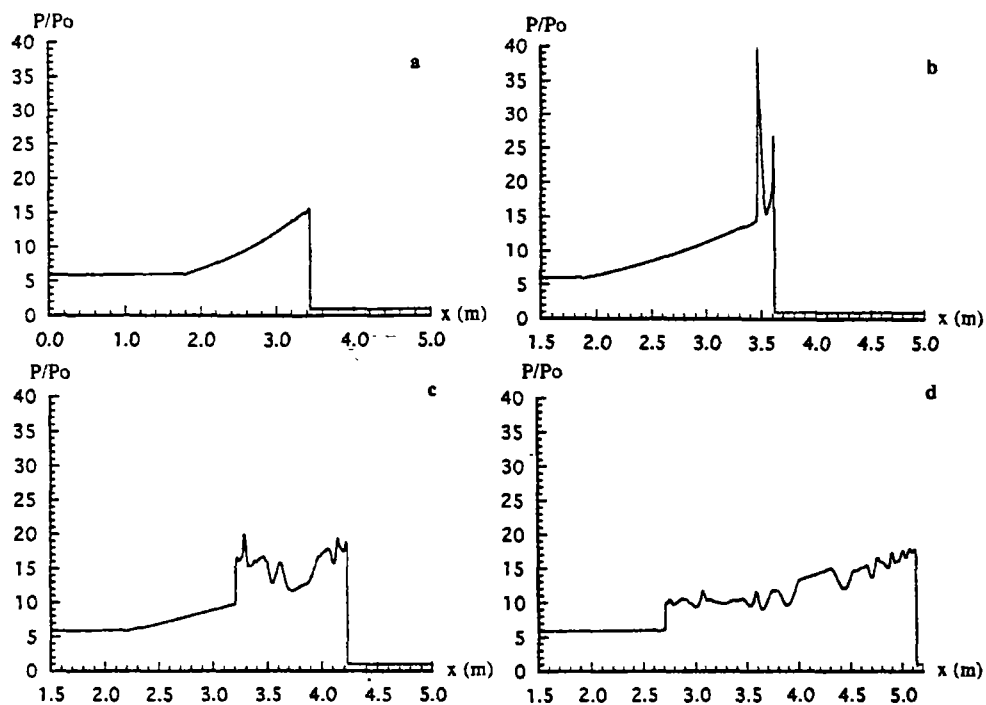
102

Fig.4 Sequential pressure profiles along the axis of symmetry of case one with a 30° converging angle

section is helpful to increase the flow pressure behind the detonation front and produce a more uniform driving flow.

4.2 Detonation driver with a 45° convergence angle

From the numerical simulation of case one, the driving flow is known to be improved, but the flow pressure between positions at 2.7 m and 4.0 m, as shown in Fig. 4d, is still lower than that behind the detonation front. This means that an even stronger upstream-travelling shock wave is required. So, case two is designed by setting the convergence angle to be 45° in type A as shown in Fig. 2. The idea put into this case is that a larger reflection angle may induce a stronger upstream travelling shock wave. Numerical results of case two are presented in Figs. 5 and 6.

In Figs. 5 and 6, the wave interactions so far observable appear to be similar to those shown in Figs. 3 and 4. However, some features different from case one are worth pointing out. The stronger shock reflection generated as shown in Fig. 5b results in a stronger upstream travelling shock wave. Therefore, a higher peak pressure due to shock wave focusing is observable in the pressure distribution of Fig. 6b, which is 25% higher than that in Fig. 4b. The post-shock pressure behind the upstream-travelling shock wave in Fig. 6d is 10% higher than that in Fig. 4d. This is useful for generating uniform driving flows. By examining the peak pressure at the detonation front in Figs. 4d and 6d, the peak pressure in Fig. 6d is
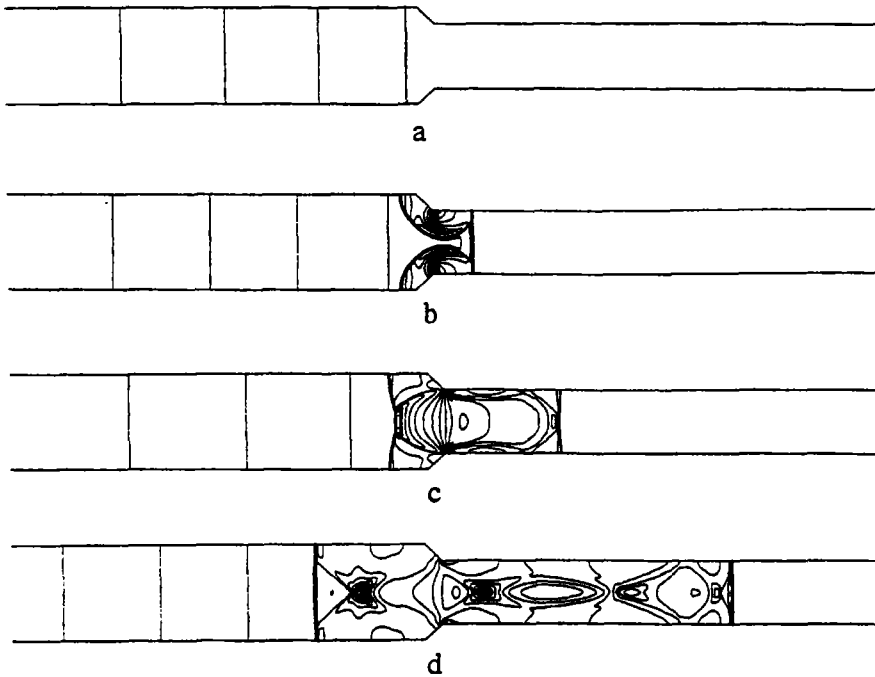
103

Fig.5 Time sequences of isobars of the flow motion showing wave interactions in case two with a 45° converging angle

lower. This means the detonation front in case two is less overdriven. From the viewpoint of the uniformity of driving flows, it could be recognized that a less overdriven-detonation front will benefit the detonation driver and produce a more uniform driving flow.

From the numerical result it is understood that the configuration of case two is better than case one. This is attributable to the larger convergence angle that can induce a stronger upstream travelling shock wave which is favorable to the generation of a more uniform flow pressure.

4.3 Detonation driver with a 90° convergence angle

Motivated by observations in the last two cases, the third case is so designed with a 90° convergence angle that a much stronger upstream travelling shock wave could be obtained. The configuration of case three is taken to be type B as shown in Fig. 2b, actually it is the same as type A with a 90° convergence angle. Four sequential isobars of the wave interaction near the area-changing section are presented in Fig. 7, and the sequential pressure distributions along the axis of symmetry are plotted in Fig. 8.

It would be helpful to examine the performance of the three detonation drivers together by comparing Fig. 7 with Figs. 3 and 5, as well as Fig. 8 with Figs. 4 and 6 since their configurations are similar. In these three cases, the major wave phenomenon is that the shock wave reflects from the converging wall and focuses on the axis of symmetry, which leads to the generation of two shock waves. One is the upstream travelling shock wave as
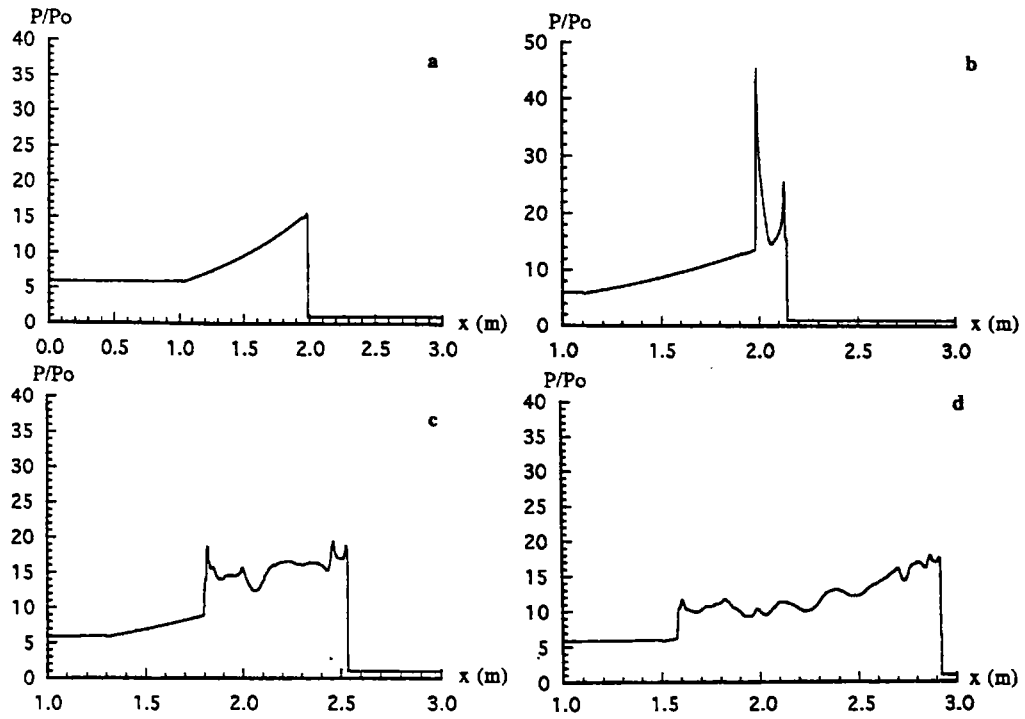
104

Fig.6 Sequential pressure profiles along the axis of symmetry of case two with a 45° converging angle
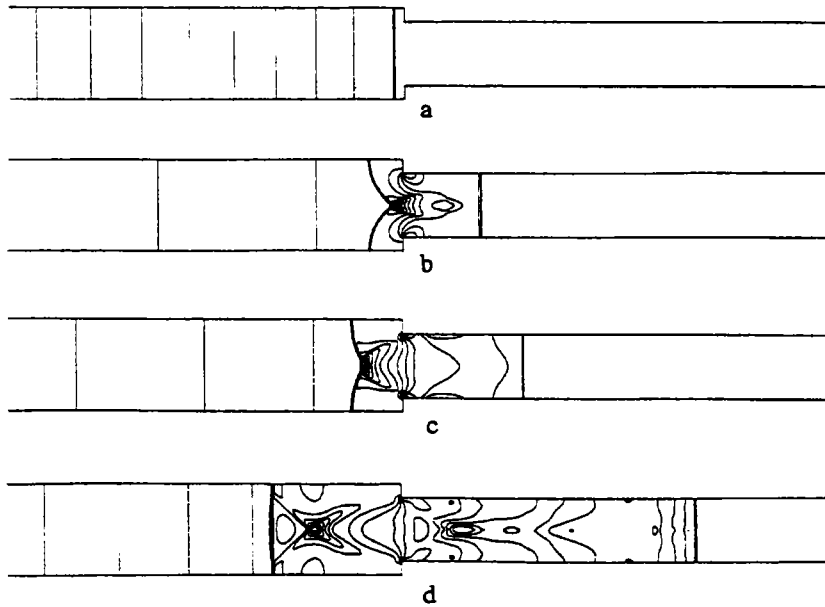

Fig.7 Time sequences of isobars of the flow motion showing wave interactions in case three with a 90° converging angle
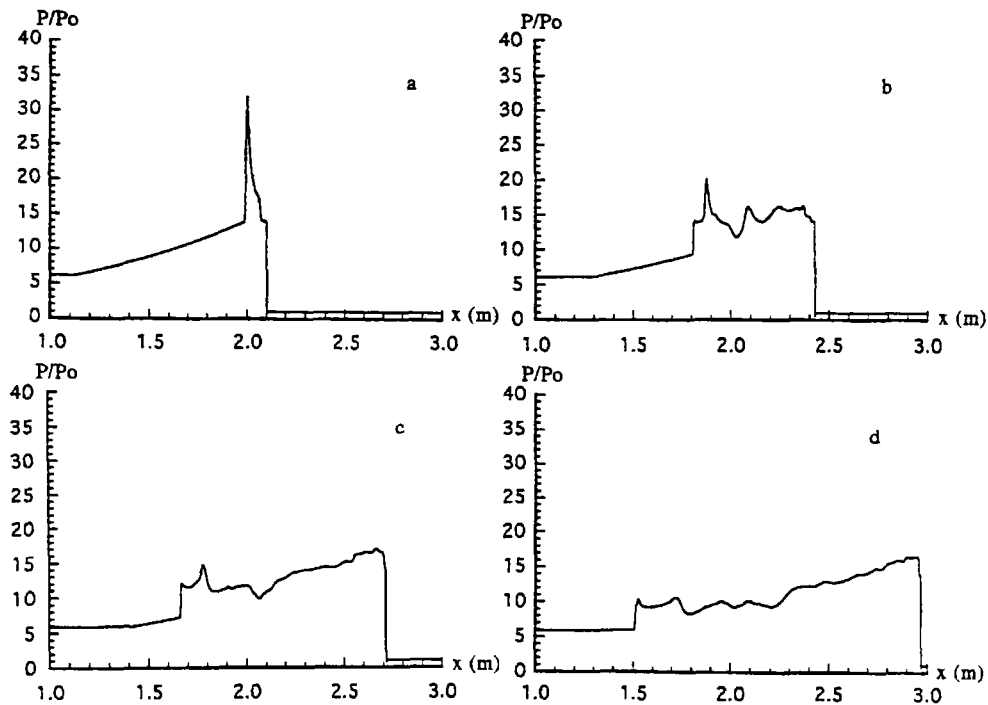
105

Fig.8 Sequential pressure profiles along the axis of symmetry of case three with a 90° converging angle

shown in Figs. 3d, 5d and 7d, which increases the pressure of the gas it processes. The stronger the shock wave is, the greater the improvement on driving flows. Another shock wave is a downstream travelling one that can catch up with the detonation front and results in an over-driven detonation front. This shock wave is difficult to observe since shock wave focusing appears just shortly behind the detonation front, but it can be identified from Figs. 4b and 6b. The over-pressure behind the detonation fronts is 27 in Fig. 4b and 24 in Fig. 6b. Both are higher than the C-J pressure of 16 in Figs. 4a and 6a. This results from the interaction of the downstream travelling shock wave with the detonation fronts. The over-driven detonation front will attenuate gradually since it is not self-sustained, but the driving flow uniformity will be affected in some extent.

By examining the numerical results of the three test cases, it is found that from case one to three, the upstream travelling shock wave becomes stronger and stronger, and the detonation front gets less and less over-driven. The difference between case one and two is obvious, but is minor between case two and three. Moreover, the increase of the post-shock pressure behind the upstream travelling shock wave is not easy to identify from Figs. 6d and 8d, but the detonation front in case three appears to be not as much over-driven as in case two. Therefore, the pressure profile in Fig. 8d appears more favorable, which is achieved by avoiding the over-driven detonation front. A key mechanism in these three cases with different convergence angles is the amount of transverse shock reflections. As the angle
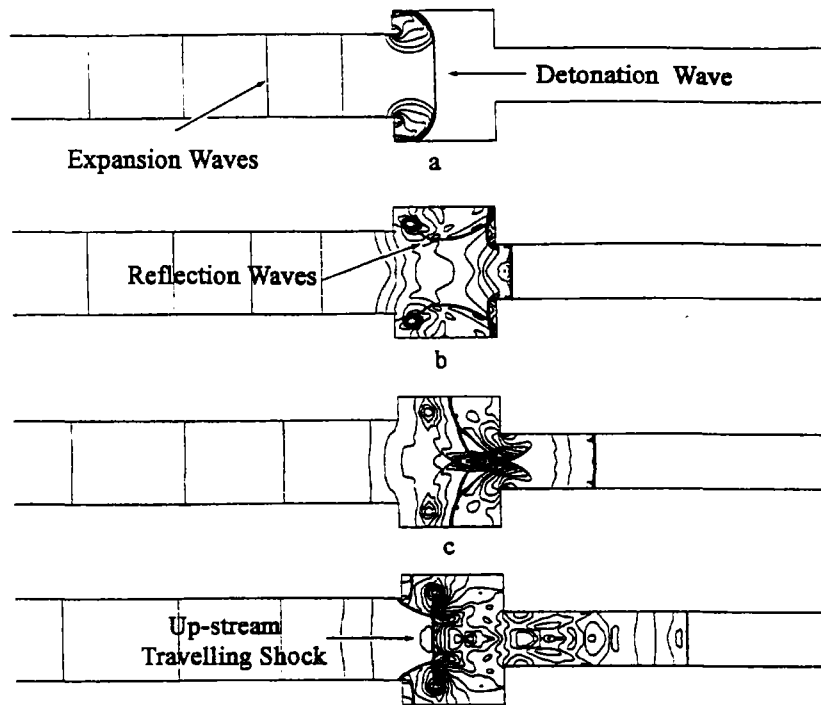
106

Fig.9 Time sequences of isobars of the flow motion showing wave interactions in case four with a cavity ring

increases, the component of the transverse reflections decreases. In the limit, as the angle becomes 90°, there is little or no transverse reflection, and the reflections are all axial and in the upstream direction only. This is reason that the flow state appears the cleanest and the detonation front is less overdriven in Fig. 8d.

In conclusion, the generation of a stronger upstream travelling shock wave and a less over-driven detonation front in a detonation driver is the key to creating high quality driving flows.

4.4 Detonation driver with a cavity ring

Although the numerical results presented in the previous three cases show much improvement of driving flow uniformity, the post-shock pressure behind the upstream travelling shock wave is still lower than the C-J pressure. In order to improve further the detonation driver performance, the configuration of type C, as shown in Fig. 2, is studied in case four. The diameter ratio of the large diameter tube to the cavity ring and to the small diameter tube is taken to be 1.5:2.5:1.0. It is expected that this special configuration could be useful to avoid the over-driven detonation as well as to produce a stronger upstream travelling shock wave. Numerical results of this case are given in Figs. 9 and 10.

Sequential isobars of wave interactions near the cavity ring are shown in Fig. 9. It is observed that the detonation front first diffracts at the frontal surface of the cavity ring in
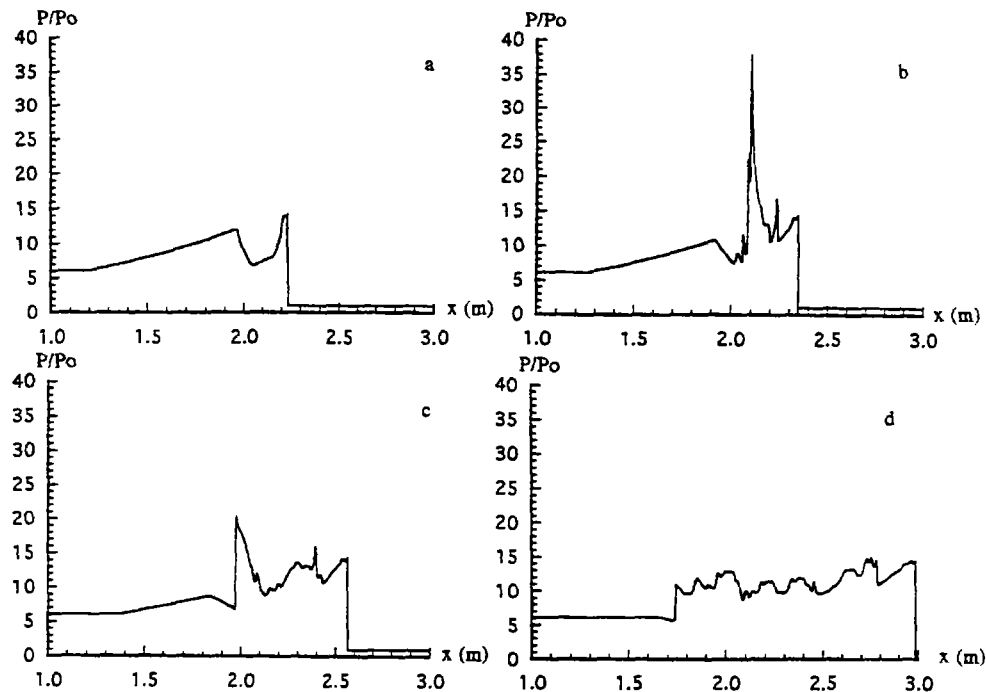
107

Fig.10 Sequential pressure profiles along the axis of symmetry of case four with a cavity ring

Fig. 9a, and then reflects from its side wall as seen in Fig. 9b. The diffracting detonation front bounces back later from the rear surface of the cavity ring as shown in Fig. 9b. Then, the reflected shock waves coalesce toward the axis of symmetry and complex wave interactions develop in the cavity ring as shown in Fig. 9c. A nearly normal shock wave is finally generated and travelling upstream as shown in Fig. 9d.

Figure 10 shows four sequential pressure distributions along the axis of symmetry. The result in Fig. 10a corresponds to the flow field in Fig. 9b at the time instant immediately after the detonation front moves out of the cavity ring. The pressure drop observable behind the detonation front is due to wave diffraction. Figure 10b shows a pressure peak generated when the coalescence of reflected shock waves appears in Fig. 9c. The pressure peak decreases very rapidly as seen in Fig. 10c and the driving flow between the upstream travelling shock and the detonation front at almost uniform pressure is obtained in Fig. 10d.

By comparing the pressure distribution in Fig. 10d with those in Figs. 4d, 6d and 8d, it is found that the induced pressure behind the upstream travelling shock wave is higher, the detonation front is less over-driven, and the driving flow appears more uniform. This demonstrates that the configuration of case four could produce a much stronger upstream-travelling shock wave and avoid an over-driven detonation front. These are achieved due to the reflection of the diffracted detonation front from the rear surface of the cavity ring. Moreover, the flow energy stored in the cavity ring is also favorable for the generation of a more uniform driving flow.
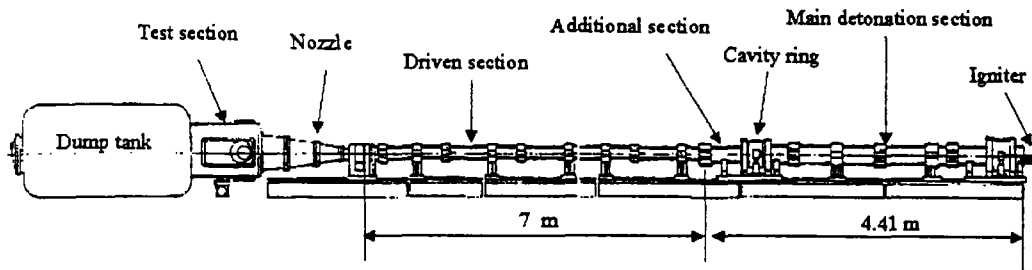
108

Fig.11 Schematic of the new detonation-driven shock tunnel installed in Institute of Mechanics, Chinese Academy of Sciences, Beijing

5 Experiments

Based on the conclusion drawn from the numerical investigations, a new detonation-driven shock tunnel, as schematically shown in Fig. 11, is manufactured and installed at the Institute of Mechanics, Chinese Academy of Sciences, Beijing. This detonation-driven shock tunnel consists of six main parts: a main detonation section, a cavity ring, an additional detonation section, a driven section, a nozzle and a dump tank. The main detonation section is 3.87 m long and 90 mm in diameter, the cavity ring is 360 mm long and 130 mm in diameter, and the additional detonation section is 180 mm long and 60 mm in diameter. The detonation driver therefore consists of these three sections. The driven section is 7 m long and 60 mm in diameter, and is also referred to as the shock tube. The length of both the additional detonation section and the cavity ring are changeable so that the optimum configuration could be explored.

Several experiments have been conducted by varying the initial pressure and mass fractions of the H_2/O_2 mixture. Stagnation pressure histories measured at the end wall of the driven section are presented to examine the uniformity of test flows. In the experiments, the shock tube is closed without a nozzle to remove the effects of the nozzle on the test gas flow. However, it is too difficult to measure the pressure profiles along the detonation driver and present them in the same manner as in the numerical simulations. Nevertheless, the stagnation pressure histories at the end wall of the shock tube could reflect the wave characteristics observed in the driving flows of the numerical simulations, for example, in Fig. 10d. The results from two experiments, as shown in Fig. 12, are obtained at the same initial condition of $P_{4i} = 0.5MPa, P_1 = 1.2KPa, H_2 : O_2 = 4 : 1$. The figure shows that the two pressure profiles are similar to each other and experimental repeatability is well demonstrated. Moreover, the two experimental results exhibit similar wave characters as observed in the pressure profile in Fig. 10d – the pressure jump appears first, showing the arrival of the leading shock wave, followed by a pressure decrease, which is also observable in Fig. 10d. And then the second pressure jump comes due to the effect of the cavity ring, and leads a uniform flow slug with pressure fluctuations, which attenuated much more than in Fig. 10d. Finally, another pressure jump appears, which is believed to be due to the reflected shock from the upstream closed end of the detonation driver. In addition, the
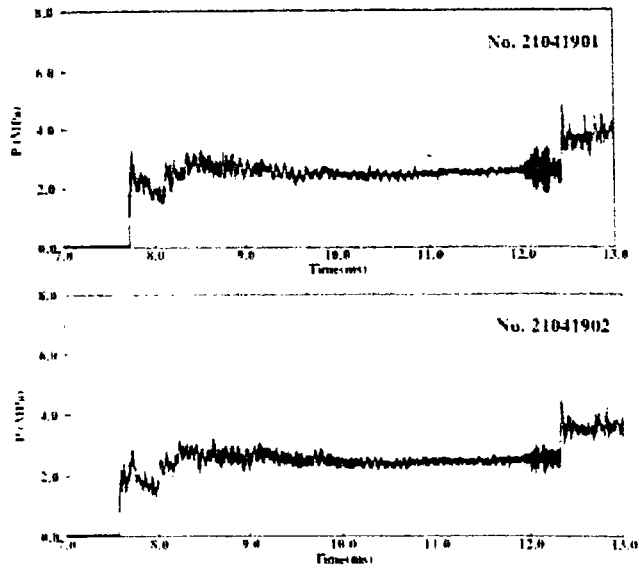
109

Fig.12 Stagnation pressure histories measured at the end wall of the driven section in case 4 with a cavity ring from two experiments at the same conditions

reservoir pressure obtained with the detonation-driven shock tunnel could be maintained for as long as 4 *ms*. Considering that the result is obtained with only a 4.41 m long detonation driver, this driving time is extremely promising.

Stagnation pressure measured at the end wall of the driven section in case 3 is given in Fig. 13. and this case is the same as case 4 without any cavity ring. By comparing this result with Fig. 8d, similar features could be observed. At first, the arrival of the leading shock wave results in a pressure jump, then follows the pressure decrease, and finally, a flow slug with an almost uniform pressure comes. By examining Figs. 12 and 13. one could see that the pressure jump behind the leading shock wave in Fig. 13 is higher than in Fig. 12. which is due to the effect of the overdriven detonation front, and as a reservoir gas flow, the flow state in Fig. 12 seems more preferable than that in Fig. 13.

These experiments confirm the conclusion drawn from the numerical simulations and the forward running detonation driver with a cavity ring has demonstrated to be a more promising choice for high-enthalpy shock tunnels.

From the point view of shock wave dynamics, the wave phenomena examined in the forward-running detonation drivers in this paper are summarized as followings: The detonation front is reflected at first in the area-changing section and then focuses on the axis of symmetry. This process results in an upstream travelling shock wave and a downstream one. The upstream travelling shock wave can increase the pressure of the flow it processes. and the downstream travelling shock wave will lead to a over-driven detonation front. To improve flow uniformity in the driver, an overdriven detonation should be avoided. because otherwise it would be difficult for the upstream travelling shock to induce a pressure level that is as high as the detonation pressure. Rather. it is more preferable to keep the pres-
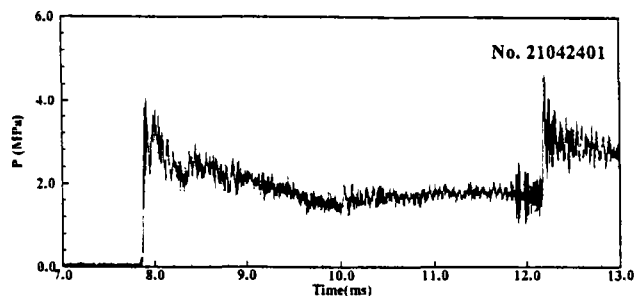
110

Fig.13 Stagnation pressure histories measured at the end wall of the driven section in case 3

sure behind the detonation from increasing (as in an over-driven wave) to achieve a uniform driving flow. In the case of the detonation driver with a cavity ring, the upstream-travelling shock wave is stronger and the downstream travelling shock wave is weaker. Moreover, the energy stored in the cavity ring can compensate for the pressure decrease due to the Taylor expansion waves. This has also been demonstrated to be helpful for the generation of a more uniform driving flow. These three wave phenomena are the key points to consider for improving the driving flow in detonation drivers.

6 Conclusions

Various detonation drivers with the specially-designed sections, operated in the forward-running model, were numerically examined in this paper. Experiments are also conducted by using a new detonation-driven shock tunnel with a cavity ring. The results are summarized as follows: the reflection of detonation waves at the converging wall results in an upstream travelling shock wave after complex wave interactions. This shock wave can increase the flow pressure which has decreased due to the trailing expansion waves. Avoiding an over-driven detonation front is also important for maintaining flow uniformity. Although the pressure fluctuations due to shock wave focusing and shock wave reflection are observable in these detonation drivers, they attenuate very rapidly as the detonation wave propagates downstream in the detonation driver and the leading shock in the shock tube. Moreover, the storage of part of the energy carried by detonation fronts in a cavity ring to compensate for the pressure decrease due to the Taylor expansion waves has demonstrated to be helpful for improving the driving flow. Among the tested detonation drivers, the configuration with a cavity ring is found to be most promising. Feasibility of the proposed detonation driver for high enthalpy shock tunnels operating in a forward-running mode is well demonstrated.

References

[1] Stalker. R.J., "An investigation of free piston compression of shock tube driver gas," Mech. Eng. Report MT-44. NRC, Ottawa, Canada, 1961.

111

[2]Stalker, R.J., "A study of the free-piston shock tunnel," *AIAA Journal*, Vol. 5, No. 12. 1967, pp. 2160-2165.

[3]Stalker, R.J., "Development of a hypersonic nozzle," *J. Roy Aeronaut. Soc*, Vol. 67, 1972, pp. 376-384.

[4]Stalker, R.J., "Hypersonic Aerodynamics in Australia," *J. British Interplanetary Soc.*, Vol. 41, 1988, pp. 611-618.

[5]Hornung, H.G., "Performance data of the new free-piston shock tunnel at GALCIT." *AIAA Paper 92-3943*, 1992.

[6]Eitelberg, G., McIntyre, T.J., Beck, W.H., and Lacey, J., "The high enthalpy shock tunnel in Göttingen, *AIAA paper 92-3955*, 1992.

[7]Itoh, K., "Tuned operation of a free-piston shock tunnel," *Procs. Of the 20 Int. Symposium on Shock Waves*, edited by B. Sturtevant, J.E. Shepherd and H.G. Hornung, Vol. I, 1995, pp. 43-51.

[8]Itoh, K., Ueda, S., Komuro, T., Saito, K., Takahashi, M., Miyajima. H. and Koga, K., "Design and construction of HIEST (High Enthalpy Shock Tunnel)," *Procs of Int. Conference on Fluid Engineering*, Vol. 1, 1997, pp. 353-358.

[9]Bird, G.A., "A note on combustion driven shock tubes," AGARD Report 146, 1957.

[10]Yu, H.R., "Shock tunnel and its application to aeroheating experiments," Thesis, Institute of Mechanics. Chinese Academy of Sciences, 1963 (in Chinese).

[11]Yu, H.R., "Experimental study of oxyhydrogen detonation driver for a shock tunnel," *Procs of 1989 Japanese National Sym on shock waves*, Sagamihara, Japan, Sept. 28-30, 1989, pp. 1-7.

[12]Yu, H.R., "Oxyhydrogen combustion and detonation driven shock tube," *Acta Mechanica Sinica*, Vol. 15, No. 2, 1999, pp. 97-107.

[13]Yu, H.R., Esser, B., Lenartz, M. and Grönig, H.,"Gaseous detonation driver for a shock tunnel," *Shock Waves*, Vol. 2, No. 4, 1992, pp. 245-254.

[14]Lu, F.K., Wilson, D.R., Bakos. R.J., and Erdos, J.D., "Recent advances in detonation techniques for high-enthalpy facilities," *AIAA Journal*, Vol. 38, No. 9, Sept. 2000, pp. 1676-1684.

[15]Chapman, D.L., "On the rate of explosions in gases," *Phil Mag*, Vol. 47, 1899, pp. 90.

[16]Jouguet, E., "Sur la propagation des reactions chimiques dans les gaz," *Journal Maths Pure Appl*, Vol. 7, 1905, pp. 347.

[17]Taylor, G.I., "The dynamics of the combustion products behind planar and spherical detonation fronts in explosive," *Proc Roy Soc A*, Vol. 200, 1950, pp. 235-247.

[18]Jiang, Z.L., Falcovitz, J. and Takayama, K., "Numerical simulations of detonation in converging chambers," *JSME International J*, Vol. 40, 1997, pp. 422-431.

[19]Jiang, Z.L., Takayama, K. and Chen, Y.S., "Dispersion conditions for non-oscillatory shock capturing schemes and its applications," *Computational Fluid Dynamics J*, Vol. 2, 1995, pp. 137-150.